Cereblon-based Bifunctional Degrader of SOS1, BTX-6654, Targets Multiple *KRAS* Mutations and Inhibits Tumor Growth

Kyle Begovich, Angela Schoolmeesters, Navin Rajapakse, Elena Martinez-Terroba, Maneesh Kumar, Arvind Shakya, Chon Lai, Steven Greene, Brandon Whitefield, Akinori Okano, Venkat Mali, Shenlin Huang, Aparajita H. Chourasia, and Leah Fung

ABSTRACT

Mutations within the oncogene *KRAS* drive an estimated 25% of all cancers. Only allele-specific *KRAS* G12C inhibitors are currently available and are associated with the emergence of acquired resistance, partly due to upstream pathway reactivation. Given its upstream role in the activation of KRAS, son of sevenless homolog 1 (SOS1), has emerged as an attractive therapeutic target. Agents that target SOS1 for degradation could represent a potential pan-*KRAS* modality that may be capable of circumventing certain acquired resistance mechanisms. Here, we report the development of two SOS1 cereblon-based bifunctional degraders, BTX-6654 and BTX-7312, cereblon-based bifunctional SOS1 degraders. Both compounds exhibited potent target-dependent and -specific SOS1 degradation. BTX-6654 and BTX-7312 reduced downstream signaling markers, pERK and pS6, and displayed antiproliferative activity in cells harboring various *KRAS* mutations. In two *KRAS* G12C xenograft models, BTX-6654 degraded SOS1 in a dose-dependent manner correlating with tumor growth inhibition, additionally exhibiting synergy with KRAS and MEK inhibitors. Altogether, BTX-6654 provided preclinical proof of concept for single-agent and combination use of bifunctional SOS1 degraders in *KRAS*-driven cancers.

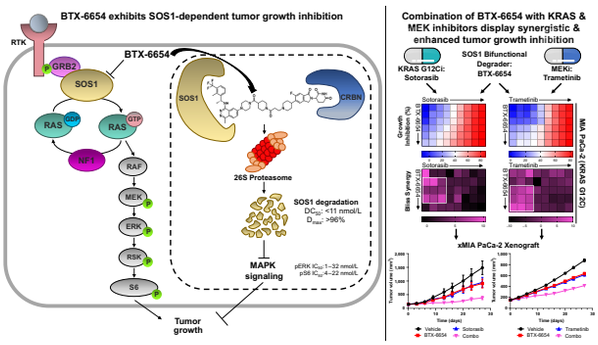

Introduction

KRAS mutations are found in approximately 20%–25% of all cancers and are heavily implicated in non–small cell lung cancers (NSCLC), pancreatic ductal adenocarcinomas (PDAC), and colorectal cancers (1). KRAS GTPase activity acts as a molecular switch alternating between an active GTP-bound state and an inactive GDP-bound state. *KRAS* mutations typically are found at G12, G13, and Q61 and favor the active GTP-bound state by impairing hydrolysis through occluding interactions with GTPase-activating proteins (G12, G13 mutants) or with the water molecule required for hydrolysis (Q61 mutants; ref. 2). Mutant *KRAS* primarily acts through the RAF/MEK/ERK pathway to promote proliferation and tumorigenesis.

Identification of a novel binding pocket in KRAS G12C proteins allowed for development of KRAS G12C allele-specific covalent inhibitors that exhibit mutant-specific antiproliferative effects in preclinical models (3). KRAS G12C inhibitors sotorasib and adagrasib have received FDA approval for use in NSCLC (4, 5). Despite the initial clinical success of these inhibitors, acquired resistance emerges, rendering them ineffective through the upregulation of receptor tyrosine kinases (RTK), RAS amplification, and the emergence of other *KRAS*-mutant alleles (6). Drug-anchored CRISPR screens and drug combination studies have identified upstream effectors of KRAS (e.g., EGFR, SHP2, SOS1) that synergize with KRAS inhibitors *in vitro* and *in vivo* (4, 7, 8).

Directly upstream of KRAS, SOS1 is the guanine nucleotide exchange factor (GEF) that interacts with KRAS to convert it from an inactive to an active state (9). While *KRAS*-mutant proteins favor the active state, they continue to cycle between GDP- and GTP-loaded states and require nucleotide exchange for subsequent activation (10). In addition, SOS1 is subject to negative feedback loops mediated by ERK phosphorylation to attenuate its GEF activity (11). Both direct and indirect functions make SOS1 an ideal target for single-agent and combination treatments. Consistent with this, genetic disruption of SOS1 resulted in tumor growth inhibition (TGI) in mutant *KRAS* xenograft models (12, 13). Recently, small-molecule inhibitors of SOS1 BI-3406 and MRTX0902, which bind to the SOS1 catalytic domain and block interaction with KRAS, displayed TGI in *KRAS*-mutant cell lines as single agents (7, 14). Combining SOS1 inhibitors with KRAS G12C or MEK inhibitors resulted in greater TGI in *KRAS*-driven xenografts.

Targeted protein degradation by proteolysis-targeting chimeras (PROTAC)/bifunctional degraders has emerged as an attractive cancer treatment modality (15). Bifunctional degraders contain a target-specific and an E3 ligase-specific ligand connected through a linker, allowing for ternary complex formation and subsequent ubiquitination and proteasome-mediated target degradation. This target removal abrogates both enzymatic and nonenzymatic functions of the protein,

BioTheryx, Inc., San Diego, California.

Corresponding Author: Kyle Begovich, BioTheryx, Inc., 5871 Oberlin Drive, San Diego, CA 92121. E-mail: kbegovich@biotheryx.com

Mol Cancer Ther 2024;23:407–20

doi: 10.1158/1535-7163.MCT-23-0513

allowing for greater potency than inhibition alone. SOS1 is a potential candidate for degradation-based therapeutics as current SOS1 inhibitors target only the catalytic domain but not its allosteric and putative RAC-GEF domains (16, 17). Recent reports have highlighted two VHL-based SOS1 degraders providing TGI in *KRAS*-mutant xenografts (18, 19). In addition, the synthesis of cereblon-based SOS1 degraders with antiproliferative effects at micromolar concentrations in colorectal cancer cell lines has been reported previously (20).

Here we describe the development of SOS1 degraders BTX-6654 and BTX-7312, which utilize cereblon as their E3 ligase target. These compounds exhibited rapid, potent, and specific degradation of SOS1, translating into downstream pathway inhibition and reduction in cell viability in a variety of *KRAS*-mutant cancer cell lines. Both SOS1 degraders synergized with RTK, mutant-specific KRAS, and MEK inhibitors in proliferation assays. BTX-6654 degraded SOS1 with > 85% in *KRAS*-mutant xenograft models resulting in TGI. Enhanced TGI was observed when BTX-6654 was combined with the KRAS G12C inhibitor, sotorasib, and the MEK inhibitor, trametinib. Together, these results demonstrate the potentiality of SOS1 degraders as therapeutic agents in *KRAS*-driven cancers, both as single agents and in combination regimens.

Materials and Methods

Synthesis of BTX-6654 and BTX-7312

Compound syntheses and characterization are described in Supplementary Materials and Methods.

Cell lines, cell culture, and other compounds

A complete list of the cell lines, source of purchase, and media used in this study is shown in Supplementary Table S1. Cell lines were authenticated by the providers using short tandem repeat profiling and routinely tested for the presence of *Mycoplasma* using the MycoAlert Mycoplasma Detection Kit (Lonza). Cells were cultured at 37°C and 5% CO_2, except for SW620, SW837, and SW1573, which were grown under 0% CO_2, and were kept in culture for no longer than 1.5 months. Sotorasib (Bioduro-Sundia), MRTX1133 (ref. 21; MedChemExpress), trametinib (ref. 22; SelleckChem), afatinib (ref. 23; MedChemExpress), CC-220 (ref. 24; MedChemExpress), MG132 (ref. 25; Bio-Techne), and MLN4924 (ref. 26; Bio-Techne) were dissolved in DMSO at 30 mmol/L stock concentrations and stored at −20°C. SOS1 degraders, ligands, and N-methyl versions were synthesized by Bioduro-Sundia and prepared as described above.

Immunoblotting

For two-dimensional (2D) assays, cells were plated in standard tissue culture-treated 12-well plates and allowed to adhere overnight. The following day, cells were treated with DMSO (control) or the indicated compounds and doses for predetermined times. Lysates were harvested in RIPA Lysis buffer containing protease and phosphatase inhibitors (Thermo Fisher Scientific Pierce RIPA Lysis Buffer; Halt Protease Inhibitor Cocktail; and Halt Phosphatase Inhibitor Cocktail). For three-dimensional (3D) assays, cells were plated in 24-well AggreWell 400 Microwell Culture plates (StemCell Technologies) prerinsed with anti-adherence rinsing solution (StemCell Technologies) in culturing media. After overnight incubation, media was removed and replenished with media containing DMSO (control) or the compound for predetermined times. Lysates were harvested in RIPA Lysis buffer containing protease and phosphatase inhibitors, stored at –80°C, and quantified using Bio-Rad *DC* Protein Assay. Loading samples were prepared in Lithium Dodecyl Sulfate (LDS) Sample Buffer (Invitrogen) and 10% final concentration of 2-mercaptoethanol (MilliporeSigma).

Samples (15 μg) in 4%–12% Bis-Tris SDS-PAGE gels were run in 1× MOPS SDS buffer, followed by wet transfer to nitrocellulose membrane using 20% methanol in 1× transfer buffer for 75 minutes at 110 V. Blots were blocked with Intercept blocking buffer (LI-COR Biosciences) for 1 hour at room temperature. Primary antibody was prepared in blocking buffer and incubated overnight at 4°C. All antibodies are listed in Supplementary Table S2. The following day, blots were washed with 0.1% PBS-Tween and incubated with secondary antibody diluted in blocking buffer for 1 hour at room temperature protected from light. Blots were washed with 0.1% PBS-Tween and imaged on the LI-COR Odyssey CLx Imager. Signals for each protein were determined using Image Studio 5.2. Proteins were normalized to β-actin as loading control. Phosphorylated proteins were normalized to the respective total protein signals. Changes in signals were represented as % of DMSO by taking the signal ratio of treatment normalized signal to DMSO normalized signal. Relative IC_{50}s were used to calculate the IC_{50} values for phospho-ERK (pERK) and phosphoribosomal protein S6 (pS6).

Cereblon with SOS1 ternary complex formation alphascreen assay

The N-term Flag-2xStrepII tagged full-length human cereblon bound to full-length human C-term HA-His-tagged DDB1 was purified. The N-term GST-tagged SOS1 exchange domain was purchased (Cytoskeleton, Inc.). Ternary complex formation of GST-SOS1and FLG-cereblon/His-DDB1 mediated by SOS1 degraders was measured using PerkinElmer AlphaScreen Technology. SOS1 degraders or final 0.5% DMSO carrier were titrated and incubated with final concentration of 2 nmol/L GST-SOS1 and 12 nmol/L FLAG-cereblon/His-DDB1 in 50 mmol/L HEPES pH 7.3, 50 mmol/L NaCl, 0.005% Brij35, 1 mg/mL BSA, 0.5 mmol/L TCEP assay buffer. Titrated SOS1 degraders or DMSO were incubated with GST-SOS1 and FLAG-cereblon/-His-DDB1 for 20 minutes before final concentration of 20 μg/mL of both nickel chelate AlphaScreen donor beads and anti-GST AlphaScreen acceptor beads were added. After 90 minutes, AlphaScreen signal was measured (680 nm excitation; 520–620 nm emission), using BMG ClarioStar AlphaScreen reading protocol. Data curves and EC_{50}s were processed via ActivityBase (IDBS).

SOS1 and K-RAS4B alphascreen binding assay

The N-term GST-tagged SOS1 exchange domain and N-term His-tagged K-RAS4b were purchased (Cytoskeleton). SOS1 inhibitors or degraders or final 0.5% DMSO carrier were titrated and added to 60-nmol/L final concentration of His-KRas4B with 2-μmol/L GTP in 50-mmol/L HEPES pH 7.3, 50-mmol/L NaCl, 0.005% Brij35, 1 mg/mL BSA, 0.5-mmol/L TCEP, 5-mmol/L $MgCl_2$ assay buffer. Then 5-nmol/L final concentration of GST-SOS1 was added. After 20 minutes, final concentration of 20 μg/mL of both glutathione AlphaScreen donor beads and nickel chelate AlphaScreen acceptor beads were added. After 90 minutes, AlphaScreen signal was measured and data were processed as described above.

HiBiT assay

HiBiT cell lines (Promega) were plated in 384-well white-walled, clear-bottom plates and incubated overnight. The following day, cells were treated in 10-point dose–response curves in duplicate wells using the Tecan D300e Digital Dispenser for 6 hours (GSPT1-, Ikaros-, and Aiolos-HiBiT lines) or 24 hours (SALL4-HiBiT line). HiBiT levels were determined by adding Nano-Glo HiBiT Lytic Reagent. Plates were

then scanned for luminescence measurement on the CLARIOstar Plus. Dose–response curves were represented as % of DMSO.

Proteomics assay

LoVo cells were treated with DMSO, 200-nmol/L BTX-6654 or BTX-7312 for 6 hours and lysed in 8-mol/L urea, 50 mmol/L ammonium bicarbonate, and benzonase. Extracted proteins were digested with trypsin/Lys-C mix (Promega), acidified with formic acid and desalted using AssayMap C18 cartridges mounted on an AssayMap Bravo Platform (Agilent Technologies). Peptide concentration was determined using a NanoDrop spectrophotometer (Thermo Fisher Scientific) and 30 μg of total peptide was used for Tandem Mass Tag (TMT) labeling at a 3:1 TMT-to-peptide (w/w) ratio and dried down using a SpeedVac concentrator. Dried peptide fractions were reconstituted with 2% acetonitrile, 0.1% formic acid and analyzed by LC/MS-MS using a Proxeon EASY nLC system (Thermo Fisher Scientific) coupled to an Orbitrap Fusion Lumos mass spectrometer equipped with FAIMS Pro device (Thermo Fisher Scientific). All mass spectra were analyzed with SpectroMine software (Biognosys) using the TMTpro default settings against the Uniprot human database (reviewed entries) downloaded in April 2022. "MSstatsTMT Report" file generated by SpectroMine was used to detect differentially abundant proteins using R package MSstatsTMT (v2.8.0; ref. 27). Protein summarization and normalization were performed, followed by testing for differential protein abundance across experimental conditions.

Generation of knockout cell lines (cereblon, SOS1, and SOS2)

CRISPR-Cas9 system was used to generate cereblon, SOS1, and SOS2 knockouts (KO). Target-specific crRNAs (cereblon: AAAATCCTGTTCTTCTCGAT, SOS1: GCATCCTTTCCAGTGTACTC, SOS2: GAGAACAGTCCGAAATGGCG) were annealed to tracrRNA (IDT) to generate guide RNAs (gRNA). The RNP complex were assembled by mixing cas9 nuclease (IDT) with gRNAs and nucleofected along with Alt-R cas9 electroporation enhancer (IDT) into their respective cell lines using SF Cell Line 4D-Nucloefector X Kit (Lonza), 4D-Nucleofector Core Unit (Lonza) and X Unit (Lonza). KO clones were grown from single colonies for SOS1 KO cell lines whereas KO pools were utilized for cereblon and SOS2 KO cell lines. All KO cell lines were confirmed by immunoblotting.

H358 SOS1-binding mutant cell line generation

N-terminally 3xFLAG-tagged SOS1 [wild-type (WT), H905V, and N879A/H905V] plasmid constructs were designed and purchased (VectorBuilder). Lenti-X HEK293T (Takara Bio) cells were transfected with plasmids using Lenti-X Packaging Single Shots (Takara Bio). Supernatants were collected 48 hours after transfection and concentrated using Lenti-X Concentrator (Takara Bio). H358 SOS1 KO cells were transduced with lentivirus with polybrene and selected in media containing 1 μg/mL puromycin (Sigma-Aldrich). Lentiviral expression was confirmed with immunoblotting.

Cell viability assays

For 2D cell viability assays, cells were plated and incubated overnight in 96-well white-walled, clear-bottom plates (Perkin Elmer) for EBC-1, NCI-H358, MIA PaCa-2, HEK293 and normal human lung fibroblast (NHLF) cells or 384-well white-walled, clear-bottom plates (Thermo Fisher Scientific) for K562 cells. The following day, cells were treated in 9-point dose–response curves in duplicate wells using the Tecan D300e Digital Dispenser and incubated for 3 days at 37°C. Cell viability was determined by adding CellTiter-Glo 2.0 Cell Viability Assay (Promega). Plates were then scanned for luminescence measurement on the CLARIOstar Plus. Dose–response curves were represented as % of DMSO generated using the four parameters variable slope in GraphPad Prism 9. SOS1 degrader-sensitive cells were defined as those displaying ≥30% reduction in cell viability with relative IC_{50} values <150 nmol/L.

For 3D cell viability assays, cells were plated and incubated for 1–2 days (depending on the cell line) in 96-well black-walled, clear round-bottom, ultra-low attachment plates (Corning). Following initial incubation, cells were treated in 9-point dose–response curves in duplicate wells using the Tecan D300e Digital Dispenser and incubated for 5–6 days at 37°C to allow for at least two cell doubling times. Cell viability was determined by adding CellTiter-Glo 3D Cell Viability Assay (Promega). Luminescence measurements and IC_{50} value calculations were determined as described above.

Drug combination assays

Cells were plated as described above and cotreated with BTX-6654 or BTX-7312 and sotorasib or MRTX1133 or trametinib or afatinib in duplicate. Defined compound concentrations were determined by the IC_{50} of each compound and establishing doses where drugs had negligible to maximal potency on cell viability in a 5×8 matrix. Cell viability was measured using CellTiter-Glo 3D Cell Viability Assay. Bliss and Loewe analysis was conducted using SynergyFinder 3.0 software, with highly synergistic interactions displaying scores greater than +10 (28). Most synergistic area (MSA) values represent the average values of a 3×3 portion of the matrix for all drug combinations. The maximum fold change in RAS pathway inhibitor IC_{50} was determined by dividing the inhibitor-alone IC_{50} by the IC_{50} value of the inhibitor in combination with a defined concentration of SOS1 degrader. Synergy between two drugs was defined by two factors: a value >10 for the MSA in either Bliss or Loewe synergy analysis and a >3-fold reduction in IC_{50} of the RAS pathway inhibitor when used in combination.

Pharmacokinetic studies in mice

Balb/c nude female mice (Beijing Vital River Laboratory Animal Technology Co.) were given either a bolus intravenous or intraperitoneal dose in 10% captisol in 50-mmol/L citrate buffer pH 5.0 buffer. Blood samples were obtained by retro-orbital bleed while the animals were anesthetized with isoflurane or by terminal cardiac puncture. In studies in which tumor samples were collected, blood was collected by terminal cardiac puncture after animals were euthanized with CO_2. Blood samples were collected at the indicated times in tubes containing K_2EDTA as anticoagulant. Samples were centrifuged within 1 hour of collection and plasma was collected, diluted 1:1 with 25-mmol/L citrate buffer (pH 1.5) and stored at –80°C until analysis. Total compound concentrations were determined by LC/MS-MS. Where tumor concentration was determined, tumors were collected from 4 animals at each timepoint, weighed, and stored at –80°C until analysis. Tumor homogenate concentrations were converted to tumor concentrations to calculate tumor-to-plasma ratios. All *in vivo* studies were approved and performed in accordance with the local guidelines of the Institutional Animal Care and Use Committee.

Xenograft models

Efficacy studies were performed using NCI-H358 and MiaPaCa-2 models. For the combination studies, xMiaPaCa-2 cells were utilized. 6 to 8 weeks old female Balb/c nude mice were inoculated subcutaneously with either NCI-H358 (5×10^6 with matrigel), MiaPaCa-2 (10×10^6 with matrigel) or xMiaPaCa-2 (10×10^6 with matrigel) cells in the right flank. Dosing started when the tumor volume reached

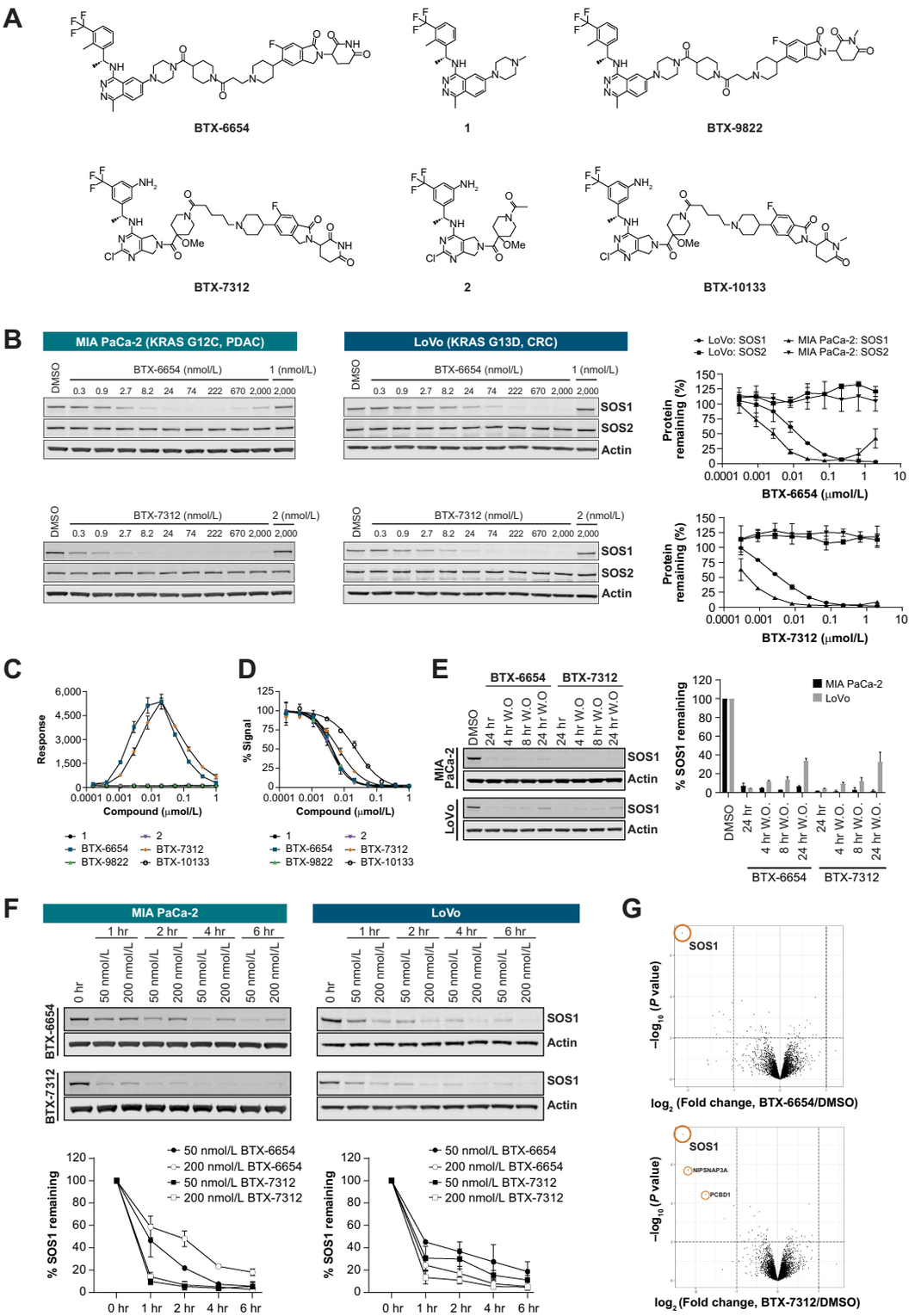

Figure 1.

BTX-6654 and BTX-7312 are potent, rapid, and selective degraders of SOS1. **A,** Chemical structures for bifunctional cereblon-SOS1 degraders BTX-6654 and BTX-7312, their respective ligands 1 and 2 as well as N-methyl versions BTX-9822 and BTX-10133. **B,** Left, Immunoblot analysis for SOS1 and SOS2 after treatment of BTX-6654, BTX-6608 (2 μmol/L), BTX-7312 or BTX-9799 (2 μmol/L) at the indicated doses for 24 hours in MIA PaCa-2 and LoVo cells. Right, Line graph quantification of SOS1 and SOS2 from immunoblots. **C,** Cereblon-SOS1 ternary complex formation analysis by AlphaScreen of the indicated compounds.

(*Continued on the following page.*)

approximately 150 mm^3. Tumor volumes and body weights were measured twice weekly. Plasma and tumor samples were collected at the end of study for pharmacokinetic and pharmacodynamic analysis.

Statistical analysis

All data are presented as mean ± SD unless mentioned otherwise. Statistical significance was assessed by the two-tailed *t* test using GraphPad Prism 8.0 software. Differences were considered statistically significant at *, $P < 0.05$; **, $P < 0.01$; ***, $P < 0.001$.

Data availability statement

The data generated in this study are available in the article and its Supplementary Data files.

Results

SOS1 degradation by BTX-6654 and BTX-7312 is rapid and specific

BTX-6654 and BTX-7312 (**Fig. 1A**) were leads from initial screening to identify bifunctional SOS1 degraders. These utilized two different precedented target-binding ligands based on the phthalazine (**1**, BTX-6654; ref. 29) or pyrrolopyrimidine (**2**, BTX-7312; ref. 30) scaffold with a 6-fluoro isoindoline cereblon binding moiety. Both ligands represent SOS1 inhibitors. Treatment of BTX-6654 and BTX-7312 for 24 hours in MIA PaCa-2 (*KRAS* G12C, PDAC) cells resulted in a maximum SOS1 degradation (D_{max}) up to 96% and half-maximal degradation concentration (DC_{50}) values of 2.4 and 0.5 nmol/L, respectively (**Fig. 1B**). LoVo (*KRAS* G13D, colorectal cancer) cells treated with SOS1 degraders displayed up to 97% SOS1 degradation and DC_{50} values of 10.1 nmol/L (BTX-6654) and 3.9 nmol/L (BTX-7312; **Fig. 1B**). Like other bifunctional protein degraders, BTX-6654 displayed a minor hook effect in MIA PaCa-2 cells, with SOS1 degradation decreasing at higher concentrations due to saturation of cereblon or SOS1 binding sites, lowering the ability to form ternary complexes. The lack of a hook effect in BTX-6654-treated LoVo cells stems from differences in expression levels of the bifunctional degrader substrates. Lower expression levels of either or both substrates are more likely to demonstrate a hook effect because the binding sites reach saturation quicker. Consistent with this notion, analysis from the Cancer Dependency Map (DepMap) Portal (31) revealed that cereblon and SOS1 levels [$\log_2$(transcripts per million +1)] were lower in MIA PaCa-2 (3.9, 2.7) compared with LoVo (4.2, 3.9), respectively. In addition, no hook effect was observed with BTX-7312 up to 2 μmol/L in both cell lines, with SOS1 remaining nearly completely degraded across a wide range of concentrations. The lack of hook effect with BTX-7312 suggests that this degrader demonstrates higher cooperative efficiency over BTX-6654 with the ternary complex formation outcompeting the individual binary complex formation better with BTX-7312 (32). This prevents saturation of the binary complexes, and no hook effect is observed. Both compounds displayed similar EC_{50}s for ternary complex formation and IC_{50} values for SOS1 binding, as measured by AlphaScreen assays (**Fig. 1C** and **D**; Supplementary Table S3).

Stable, long-lived protein targets with slow resynthesis rates are particularly susceptible to the extended effects of protein degradation. Because SOS1 half-life is >18 hours (33), drug washout experiments were performed to track its resynthesis over time. SOS1 was efficiently degraded following a 24 hours treatment and remained completely degraded 24 hours after washout with both BTX-6654 and BTX-7312 in MIA PaCa-2 cells, whereas SOS1 levels rose to approximately 35% relative to the DMSO control in LoVo cells (**Fig. 1E**). On the basis of these results, we anticipate that SOS1 re-expression would take 48–72 hours after washout to reach basal levels in LoVo cells. We then determined the kinetics of SOS1 degradation with both compounds over a 6-hour time course in MIA PaCa-2 and LoVo cells. SOS1 degradation demonstrated concentration and time dependence with BTX-6654 and BTX-7312, with maximal degradation occurring at 6 and 4 hours, respectively, in both cell lines (**Fig. 1F**).

Next, we sought to determine SOS1 degrader specificity by examining SOS1 ortholog (SOS2), known complex-interactors, and neosubstrates associated with cereblon binders. Despite the high structural similarities between SOS1 and SOS2, BTX-6654 and BTX-7312 did not degrade SOS2, likely due to failed pi-interaction of SOS2 (V903) required for protein–compound interaction (**Fig. 1B**; ref. 7). In addition, SOS1 degraders failed to reduce protein levels for its known complex-interactors, EGFR, GRB2, SHP2, and KRAS (Supplementary Fig. S1A). Because cereblon binders may recruit other targets, we tested whether BTX-6654 and BTX-7312 degraded known neosubstrate targets GSPT1, Ikaros, Aiolos, SALL4, and CK1α. In HiBiT-tagged cell lines, BTX-6654 and BTX-7312 degraded approximately 65% SALL4, but left GSPT1, Ikaros and Aiolos unaffected (Supplementary Fig. S1B). While SALL4 is essential for developmental processes (34), it lacks expression in MIA PaCa-2 and LoVo cells compared with SALL4-expressing KELLY and SK-N-DZ cells (Supplementary Fig. S1C). While BTX-7312 had no effect on CK1α, BTX-6654 exhibited approximately 35% and approximately 60% CK1α degradation in MIA PaCa-2 and LoVo cells, respectively, but only concentrations much higher than its D_{max} for SOS1 (Supplementary Fig. S1D).

In addition, we performed quantitative proteomics on LoVo cells treated with BTX-6654 or BTX-7312 to identify any potential off-targets for our SOS1 degraders. SOS1 was the most significantly downregulated protein, with minimal effects on other proteins (**Fig. 1G**). Two additional downregulated proteins (NIPSNAP3A and PCBD1) were identified in BTX-7312–treated cells. NIPSNAP3A, a member of NIPSNAP family proteins, localizes to lipid rafts, but its function remains unclear and understudied (35). Loss-of-function mutations in PCBD1, a pterin-4α-carbinolamine dehydratase that can serve as a dimerization cofactor for the transcription factor HNF1α, are associated with transient neonatal hyperphenylalaninemia (36, 37). Both NIPSNAP3A and PCBD1 have no known role in cancer and the interplay between SOS1 or the RAS pathway and these proteins remains to be determined.

BTX-6654 and BTX-7312 require cereblon, the proteasome, and its target-binding site for SOS1 degradation

To confirm that SOS1 degradation depended on its E3 ligase target, cereblon, and the proteasome, we first performed a cereblon competition assay, cotreating MIA PaCa-2 and LoVo cells with BTX-6654 or

(*Continued.*) **D,** SOS1 binding analysis by AlphaScreen of the indicated compounds. **E,** Left, Immunoblot analysis for SOS1 after treatment with 200 nmol/L BTX-6654 or BTX-7312 for 24 hours and the indicated timepoints after compound washout (W.O.) in MIA PaCa-2 and LoVo cells. Right, Bar graph quantification of SOS1 protein levels from immunoblots. **F,** Top, Immunoblot analysis for SOS1 after treatment of BTX-6654 or BTX-7312 at the indicated doses for the indicated timepoints in MIA PaCa-2 and LoVo cells. Bottom, Line graph quantification of SOS1 from immunoblots. **G,** Proteomics analysis from LoVo cells treated with 200 nmol/L BTX-6654 or BTX-7312 for 6 hours. Data are represented as average ± SD of two independent experiments (**B**–**F**). Actin was used as a loading control in immunoblot analysis (**B**, **E**, **F**).

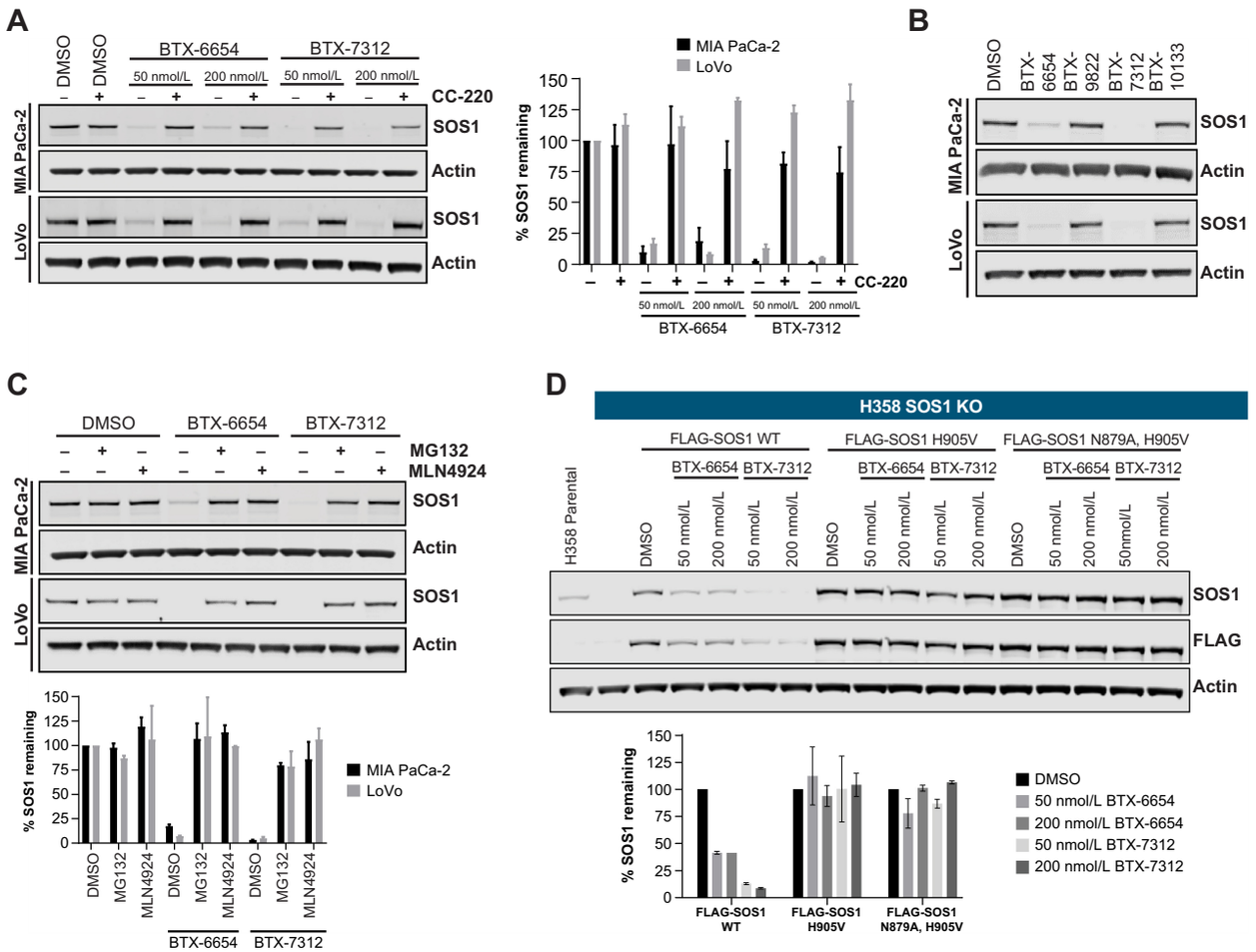

Figure 2.

SOS1 degradation by BTX-6654 and BTX-7312 are dependent on cereblon and the proteasome. **A,** Left, Immunoblot analysis for SOS1 after treatment of BTX-6654 or BTX-7312 ± CC-220 (10 μmol/L) at the indicated doses for 6 hours in MIA PaCa-2 and LoVo cells. Right, Bar graph quantification of SOS1 protein levels from immunoblots. **B,** Immunoblot analysis for SOS1 after treatment of the indicated compounds at 200 nmol/L for 6 hours in MIA PaCa-2 and LoVo cells. **C,** Top, Immunoblot analysis for SOS1 after treatment with BTX-6654 or BTX-7312 ± MG132 (10 μmol/L) or MLN4924 (1 μmol/L) at the indicated doses for 6 hours in MIA PaCa-2 and LoVo cells. Below, Bar graph quantification of SOS1 protein levels from immunoblots. **D,** Top, Immunoblots for SOS1 and FLAG after treatment of BTX-6654 or BTX-7312 at the indicated doses for 6 hours in the H358 Parental, SOS1 KO, and transgenic cell lines. Below, Bar graph quantification of SOS1 protein levels from immunoblots. Data are represented as average ± SD of two independent experiments. Actin was used as a loading control in immunoblot analysis (**A–D**).

BTX-7312 and CC-220, a cereblon-based molecular glue which outcompetes SOS1 degraders for cereblon binding at high concentrations (24). Consistent with this, SOS1 degradation was rescued upon the cotreatment of BTX-6654 and BTX-7312 in both MIA PaCa-2 and LoVo cells (**Fig. 2A**). We also utilized N-methyl glutarimide versions of BTX-6654 (BTX-9822) and BTX-7312 (BTX-10133) which lack affinity for cereblon to examine the cereblon dependency of SOS1 degradation. BTX-9822 and BTX-10133 failed to assemble cereblon-SOS1 ternary complexes (**Fig. 1C**) and prevented SOS1 degradation in MIA PaCa-2–treated and LoVo-treated cells (**Fig. 2B**). Furthermore, cotreatment of BTX-6654 or BTX-7312 with MG132 (a proteasome inhibitor) or MLN4924 (a NEDD8-activating enzyme inhibitor) blocked SOS1 degradation (**Fig. 2C**).

BTX-6654 and BTX-7312 were designed to bind to the SOS1 catalytic pocket, requiring interaction with residues N879 and H905 for binding and subsequent degradation (7, 38). To validate this mechanism, we generated transgenic cell lines stably expressing N-terminally tagged FLAG-SOS1 WT or catalytic binding mutant (H905V and N879A, H905V) constructs in NCI-H358 SOS1 KO cells and assessed SOS1 degradation. BTX-6654 and BTX-7312 degraded the FLAG-SOS1 WT protein but not the FLAG-SOS1 H905V and N879A, H905V-mutant protein, confirming that these SOS1 degraders require interactions with both residues for degradation (**Fig. 2D**).

SOS1 degradation reduces downstream signaling

Because *KRAS*-mutant cells are more sensitive to RAS pathway inhibition in anchorage-independent/spheroid (3D) than adherent (2D) culture conditions (5, 7, 39), we developed 3D immunoblot assays for MIA PaCa-2 cells to determine inhibition of downstream signaling by SOS1 degraders. BTX-6654 and BTX-7312 demonstrated low nanomolar relative IC_{50} values for pERK, pS6 (S235/S236) and phospho-AKT (pAKT S473) at 24 hours after treatment (**Fig. 3A**). Both compounds were more potent for pERK (∼4- to 15-fold IC_{50} values) and pS6 (∼12- to 18-fold IC_{50} values) inhibition than their respective

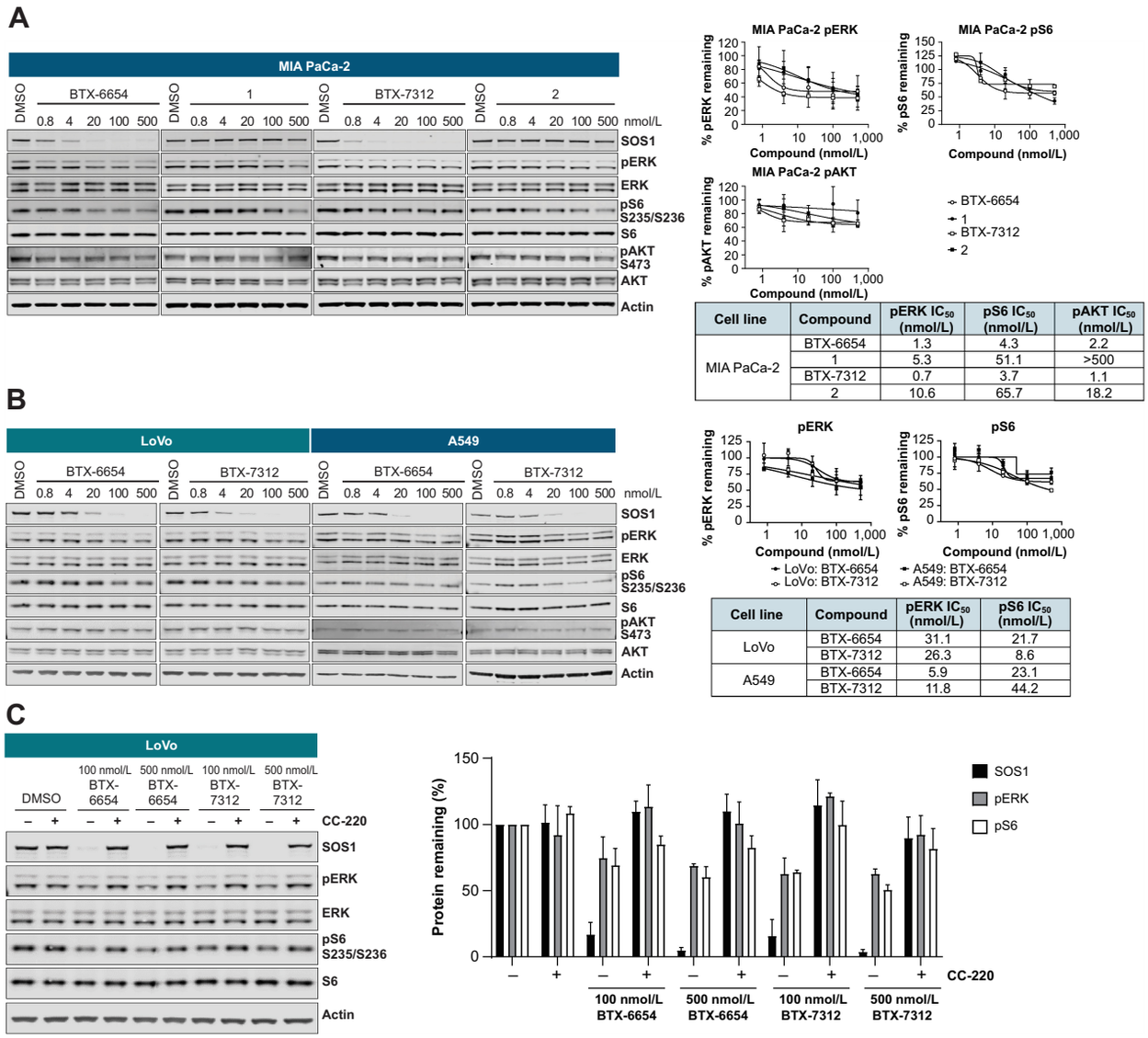

Cell line	Compound	pERK IC_{50} (nmol/L)	pS6 IC_{50} (nmol/L)	pAKT IC_{50} (nmol/L)
MIA PaCa-2	BTX-6654	1.3	4.3	2.2
	1	5.3	51.1	>500
	BTX-7312	0.7	3.7	1.1
	2	10.6	65.7	18.2

Cell line	Compound	pERK IC_{50} (nmol/L)	pS6 IC_{50} (nmol/L)
LoVo	BTX-6654	31.1	21.7
	BTX-7312	26.3	8.6
A549	BTX-6654	5.9	23.1
	BTX-7312	11.8	44.2

Figure 3.

SOS1 degradation reduces pERK and pS6 signaling in *KRAS*-mutant cell lines. **A,** Left, Immunoblot analysis for SOS1, pERK, total ERK, pS6 (S235/S236), total S6, pAKT (S473) and total AKT after treatment of the indicated compounds at the indicated doses for 24 hours in MIA PaCa-2 cells. Right, Line graph quantification of pERK and pS6 protein levels from immunoblots and their respective IC_{50} values are reported in the table. **B,** Left, Immunoblot analysis for SOS1, pERK, total ERK, pS6 (S235/S236), total S6, pAKT (S473), and total AKT after treatment of the indicated compounds at the indicated doses for 6 hours in LoVo and A549 cells. Right, Line graph quantification of pERK and pS6 protein levels from immunoblots and their respective IC_{50} values are reported in the table. **C,** Left, Immunoblot analysis for SOS1, pERK, total ERK, pS6 (S235/S236), and total S6 after treatment of BTX-6654 or BTX-7312 ± CC-220 (10 μmol/L) at the indicated doses for 6 hours in LoVo cells. Right, Bar graph quantification of SOS1, pERK, and pS6 protein levels from immunoblots. Data are represented as average ± SD of three independent experiments. Actin was used as a loading control in immunoblot analysis (**A**–**C**).

target binding ligands (compounds 1 and 2). Similarly, SOS1 degradation displayed lower relative IC_{50} values for pAKT compared with SOS1 inhibition in MIA PaCa-2 cells. BTX-6654 and BTX-7312 bound SOS1 with comparable affinities to their ligands, suggesting that the added potency is derived from SOS1 degradation rather than stronger inhibition (**Fig. 1D**). In addition, SOS1 degradation inhibited downstream signaling with IC_{50} values ranging from 5.9–31.1 nmol/L for pERK and 8.6–44.2 nmol/L for pS6 in LoVo and A549 (*KRAS* G12S, NSCLC) cells (**Fig. 3B**). pAKT was only marginally affected by SOS1 degradation, demonstrating approximately 20% maximum inhibition in these cell lines. pAKT downregulation in MIA PaCa-2 cells, but not A549 or LoVo cells, suggests that the contribution of SOS1 to pAKT signaling could be cell-type or *KRAS* mutation specific. Cotreatment of the degraders with CC-220 rescued the reduction in pERK and pS6 signaling, in LoVo cells, further demonstrating that the decrease in downstream signaling exhibited by BTX-6654 and BTX-7312 stem from SOS1 degradation, not inhibition (**Fig. 3C**). Together, these results highlight the ability of BTX-6654 and BTX-7312 to decrease pERK and pS6 signaling by degrading SOS1.

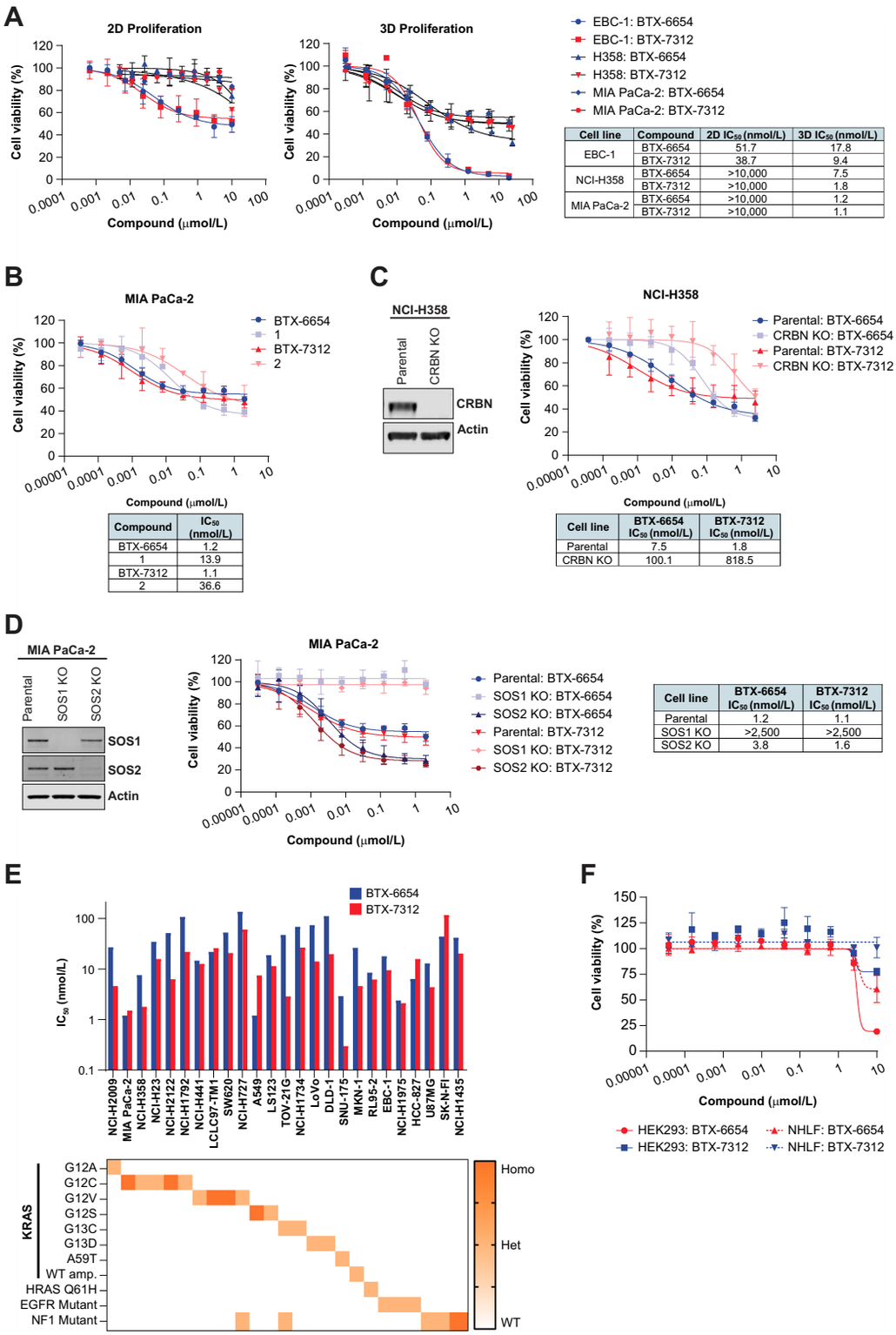

Cell line	Compound	2D IC_{50} (nmol/L)	3D IC_{50} (nmol/L)
EBC-1	BTX-6654	51.7	17.8
	BTX-7312	38.7	9.4
NCI-H358	BTX-6654	>10,000	7.5
	BTX-7312	>10,000	1.8
MIA PaCa-2	BTX-6654	>10,000	1.2
	BTX-7312	>10,000	1.1

Compound	IC_{50} (nmol/L)
BTX-6654	1.2
1	13.9
BTX-7312	1.1
2	36.6

Cell line	BTX-6654 IC_{50} (nmol/L)	BTX-7312 IC_{50} (nmol/L)
Parental	7.5	1.8
CRBN KO	100.1	818.5

Cell line	BTX-6654 IC_{50} (nmol/L)	BTX-7312 IC_{50} (nmol/L)
Parental	1.2	1.1
SOS1 KO	>2,500	>2,500
SOS2 KO	3.8	1.6

Figure 4.

BTX-6654 and BTX-7312 exhibit target-dependent antiproliferative activity in various cancer cell lines. **A,** Cell viability analysis of EBC-1, MIA PaCa-2, and H358 cells treated with BTX-6654 or BTX-7312 in dose–response under adherent (2D, left) and anchorage-independent (3D, right) conditions. IC_{50} values for each compound, cell line, and condition are reported in the table. **B,** Cell viability analysis of MIA PaCa-2 cells treated with bifunctional SOS1 degraders and their ligands in dose–response under 3D conditions. IC_{50} values for each compound are reported in the table. (*Continued on the following page.*)

SOS1 degraders exhibit cereblon- and SOS1-dependent antiproliferative effects across a variety of cancer cell types

We then evaluated BTX-6654 and BTX-7312 for their ability to inhibit cell proliferation. K562 [BCR-ABL1 fusion, chronic myelogenous leukemia (CML)] and EBC-1 (*EGFR* L858R, NSCLC) were identified via DepMap Portal (40) as SOS1-dependent cell lines. Treatment with SOS1 degraders provided IC_{50} values ranging from 1.1 to 51.7 nmol/L in proliferation assays (**Fig. 4A**; Supplementary Fig. S2B). BTX-S6654 and BTX-7312 inhibited proliferation in EBC-1 but had no effect on *KRAS* G12C-mutant NCI-H358 and MIA PaCa-2 cells under 2D conditions (**Fig. 4A**). However, when examined under anchorage-independent conditions, they robustly reduced viability in EBC-1, H358, and MIA PaCa-2 cells with IC_{50} values ranging from 1.1 to 17.8 nmol/L (**Fig. 4A**). Consistent with pERK and pS6 assays, BTX-6654 and BTX-7312 were more potent than their respective ligands, exhibiting approximately 12- and 33-fold lower IC_{50} values in MIA PaCa-2 cells (**Fig. 4B**).

To determine the cereblon dependency of BTX-6654 and BTX-7312 antiproliferative effects, we generated isogenic cell lines depleted for cereblon (cereblon KO) using CRISPR-Cas9 technology in K562 and H358 cells, with >90% KO efficiency (**Fig. 4C**; Supplementary Fig. S2). BTX-6654 displayed 9- and 12-fold higher IC_{50} values whereas BTX-7312 demonstrated 380- and 410-fold higher IC_{50} values in K562 and H358 cereblon KO, respectively, compared with parental cells. To confirm SOS1 selectivity, we generated SOS1 KO cell lines in MIA PaCa-2 cells with >95% KO efficiency. Notably, SOS1 KO cells had reduced spheroid size and cell viability compared with parental cells, highlighting the SOS1 dependence under 3D culture conditions (Supplementary Fig. S3). Upon treatment with BTX-6654 and BTX-7312, no reduction in cell viability was observed in SOS1 KO cells (**Fig. 4D**). Previous reports have suggested that SOS2 can play a compensatory role when SOS1 is blocked (7). Similarly, treatment of MIA PaCa-2 SOS2 KO cells with SOS1 degraders led to 20% greater growth inhibition compared with parental cells (**Fig. 4D**). Together, these results confirm that BTX-6654 and BTX-7312 antiproliferative activity is concordant with their proposed mechanism of action.

We then sought to identify other *EGFR-RAS-MAPK*-mutant cell lines which exhibit sensitivity to SOS1 degradation. 3D proliferation assays for multiple cell lines harboring *RAS*, *EGFR*, or *BRAF* mutations as well as cell lines with amplified WT *KRAS* were developed. We identified SOS1 degradation-sensitive cell lines with *KRAS* amplification (1/1), *KRAS* G12A (1/2), G12C (5/8), G12V (4/6), G12S (2/2), G13C (2/3), G13D (2/4), A59T (1/1), *HRAS* Q61H (1/1), *EGFR* (3/3), and *NF1* (3/4) mutations (**Fig. 4E**; Supplementary Table S4). Despite the variety of *KRAS* mutants sensitive to SOS1 degradation, none of the four *KRAS* G12D cell lines were affected. Both SOS1 inhibitors and degraders failed to meet our criteria of cell viability reduction in *KRAS* G12D cells, suggesting that these cell lines are not sensitive to SOS1 blockage (Supplementary Table S5). Consistent with lower DC_{50} values, BTX-7312 was more potent than BTX-6654 across most of the cell lines examined. However, BTX-6654 displayed a lower proliferation IC_{50} in A549 cells. This reversal is highlighted by lower IC_{50} values for both pERK and pS6 for BTX-6654 compared with BTX-7312 in this cell line (**Fig. 3B**). Finally, BTX-6654 and BTX-7312 were examined in primary and nontumorigenic cell lines to determine potential therapeutic index. SOS1 degraders only inhibited cell proliferation in HEK293 and NHLFs at 10 μmol/L and displayed IC_{50} values >5 μmol/L (**Fig. 4F**). These data suggest that SOS1 degradation has strong antiproliferative activity in a variety of *EGFR*-, *RAS*-, and *NF1*-mutant cell lines with a broad therapeutic window.

BTX-6654 treatment effectively suppresses tumor growth in *KRAS* G12C xenograft models

Because incorporating saturated heterocycles to rigidify bifunctional degrader linkers may allow for better pharmacologic profiles, we selected BTX-6654 for *in vivo* studies (41). BTX-6654 displayed favorable exposure upon intraperitoneal dosing (Supplementary Fig. S4A and S4B) and was examined in a 5-day PK-PD study in the NCI-H358 model. Plasma and tumor pharmacokinetics were evaluated at 2, 8, and 24 hours after last dose at the end of the study. BTX-6654 exposures in plasma and tumor were dose proportional at 10 and 50 mg/kg (**Fig. 5A**). Treatment of BTX-6654 resulted in >85% SOS1 degradation in tumor samples at all timepoints for both dose levels and displayed dose-dependent reductions of pERK coinciding with SOS1 degradation (**Fig. 5B** and **C**).

We then evaluated BTX-6654 in efficacy studies using NCI-H358 and MIA PaCa-2 xenograft models. Animals were treated twice daily with intraperitoneal BTX-6654 at 2 and 10 mg/kg and oral SOS1 inhibitor BI3406 at 50 mg/kg. In the NCI-H358 model, dose-dependent TGI was observed with 2 and 10 mg/kg BTX-6654 demonstrating 37% ($P < 0.01$) and 57% ($P < 0.005$) TGI, respectively (**Fig. 5D**). Tumor and plasma pharmacokinetic collection as well as SOS1 degradation were evaluated at 2, 8, and 24 hours after last dose at the end of the studies. Consistent with TGI, higher degradation correlated with higher BTX-6654 exposure levels, resulting in up to 90% SOS1 degradation (10 mg/kg) with peak SOS1 degradation at 8 hours after dosing (**Fig. 5E–G**). In the MIA PaCa-2 xenograft model, treatment with 2 and 10 mg/kg of BTX-6654 resulted in 33% ($P < 0.05$) and 43% ($P < 0.01$) tumor volume reductions, respectively (**Fig. 5H**). Pharmacokinetic and pharmacodynamic analysis of MIA PaCa-2 tumor revealed higher SOS1 degradation at higher doses, reaching 97% degradation at the 10 mg/kg dose (**Fig. 5I–K**). Both BTX-6654 dosing levels were well tolerated in both models (Supplementary Fig. S4C and S5D). In addition, the tumor concentration of BTX-6654 is sufficient to maintain suppression of SOS1. Although the modes of administration differed between BTX-6654 and BI-3406, comparable efficacies were observed in both models.

SOS1 degraders synergize with EGFR, KRAS, and MEK inhibitors *in vitro* and *in vivo*

Previous studies have reported an antiproliferative synergy effect between SOS1 inhibitors and EGFR, KRAS, and MEK inhibitors (7, 14, 42, 43). Therefore, we explored potential BTX-6654 and BTX-7312 synergy with inhibitors of *KRAS* G12C (sotorasib), G12D

(*Continued.*) **C,** Left, Immunoblot analysis for cereblon from parental and cereblon KO H358 cells. Right, Cell viability analysis of parental and cereblon KO H358 cells treated with BTX-6654 or BTX-7312 in dose–response under 3D conditions. IC_{50} values for each compound and cell line are reported in the table below. **D,** Left, Immunoblot analysis for SOS1 and SOS2 from parental, SOS1 KO, and SOS2 KO MIA PaCa-2 cells. Right, Cell viability analysis of parental, SOS1 KO, and SOS2 KO MIA PaCa-2 cells treated with BTX-6654 or BTX-7312 in dose–response under 3D conditions. IC_{50} values for each compound and cell line are reported in the table below. **E,** Top, Bar graph quantification of IC_{50} values from SOS1 bifunctional protein degrader-sensitive cell lines under 3D conditions. Below, Heat map displaying zygosity for the indicated mutations for the cell lines displayed on top. **F,** Cell viability analysis of HEK293 and NHLF cells treated with BTX-6654 and BTX-7312 in dose–response under 2D conditions. Data are represented as average ± SD of at least three independent experiments. Actin was used as a loading control in immunoblot analysis (**C**, **D**).

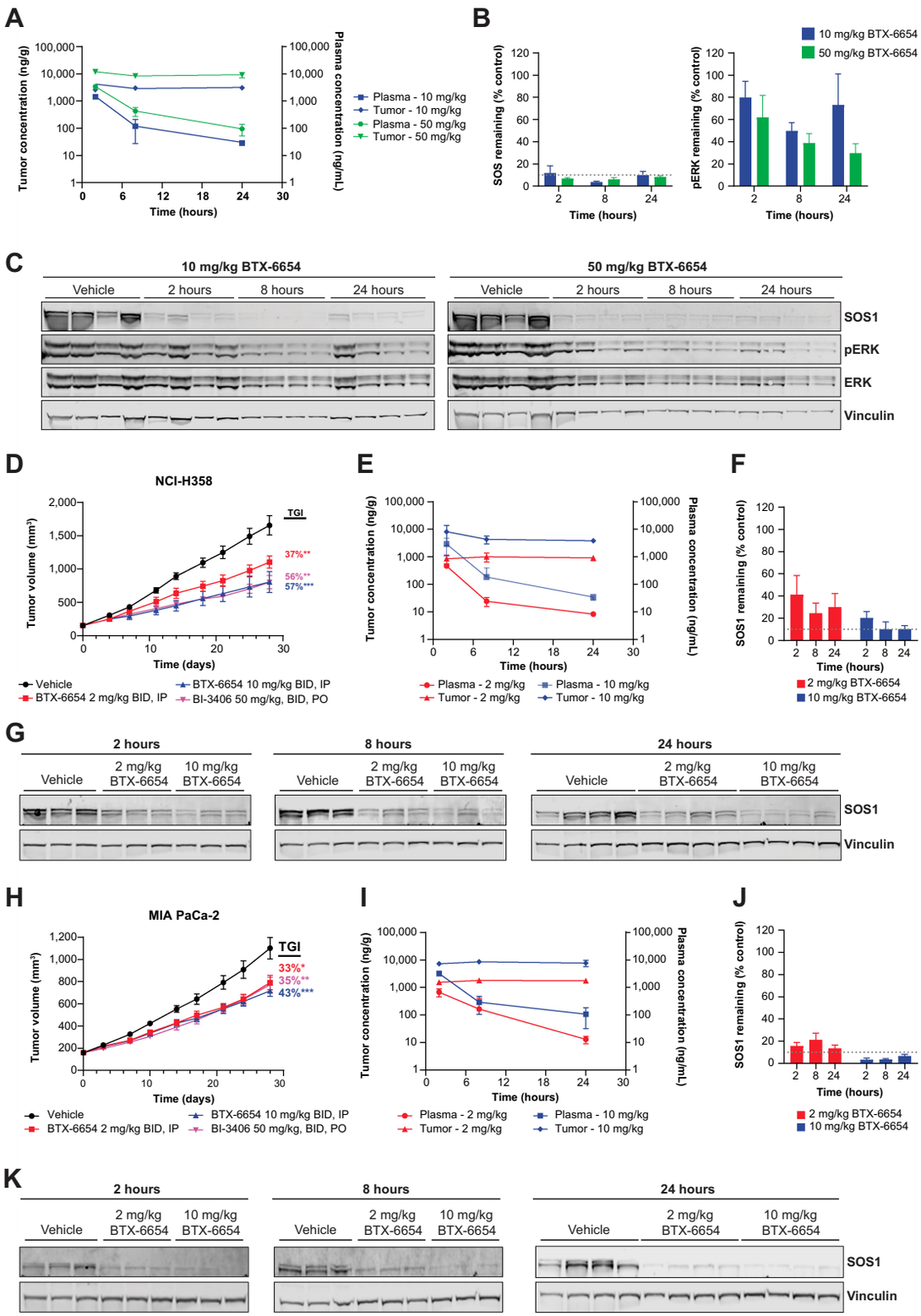

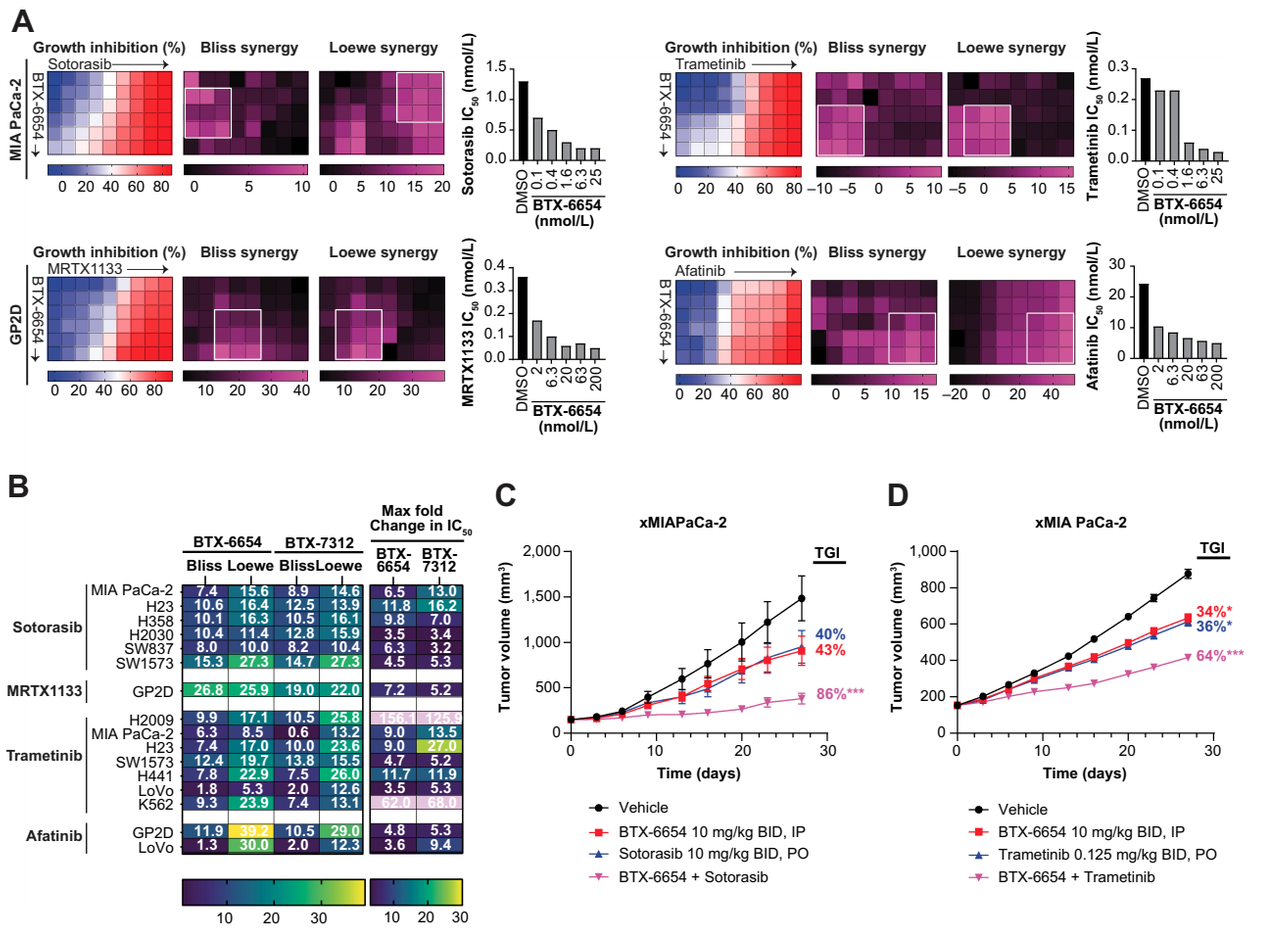

Figure 6.

SOS1 degraders demonstrate synergy with various RTK-RAS-MAPK inhibitors *in vitro* and in xenograft models. **A,** Heat maps displaying percent growth inhibition, Bliss synergy, Loewe synergy, and bar graph quantification of IC_{50} values for RTK-RAS-MAPK inhibitors with BTX-6654 in MIA PaCa-2 or GP2D cells in 3D conditions. White boxes indicate MSA. **B,** Synergy analysis of all cell lines and combinations tested with BTX-6654 and BTX-7312. Heat maps depict the MSA values for Bliss and Loewe synergy and the maximum fold change in IC_{50} values of RTK-RAS-MAPK inhibitor in combination with BTX-6654 and BTX-7312. **C,** Antitumor efficacy of BTX-6654 and sotorasib alone and in combination in xMIA PaCa-2 xenografts. **D,** Antitumor efficacy of BTX-6654 and trametinib alone and in combination in xMIA PaCa-2 xenografts. Data are represented as average of two independent experiments (**A**, **B**). Data are represented as average ± SEM from 10 mice per group (**C**, **D**). TGI, tumor growth inhibition. Statistical significance was determined with respect to the vehicle group using a two-tailed *t* test (*, $P < 0.05$; **, $P < 0.005$).

(MRTX1133; ref. 21), *MEK* (trametinib; ref. 22), and *ERBB* (afatinib; ref. 23) in 3D proliferation assays. To score for synergy, we established a threshold where the drug combination must produce a value >10 for the MSA in either Bliss or Loewe synergy analysis and reduce the IC_{50} of the RTK-RAS-MAPK inhibitor by >3-fold when used in combination. SOS1 degraders displayed synergistic effects with sotorasib, trametinib, and afatinib across multiple cell lines harboring different *KRAS* mutations (**Fig. 6A** and **B**; Supplementary Fig. S5). This was not limited to *KRAS*-mutant cells as SOS1 degradation and *MEK* inhibition demonstrated synergy in K562 cells. Notably, synergy was observed even in cell lines insensitive to SOS1 degradation alone. For example, SOS1 degraders exhibited strong synergistic scores with sotorasib and trametinib combinations in SW1573 (*KRAS* G12C) cells. Similarly, synergy was observed with MRTX1133 and SOS1

Figure 5.

BTX-6654 exhibits dose-dependent SOS1 degradation and tumor growth inhibition in *KRAS* G12C xenograft models. **A,** Plasma and tumor analysis from BTX-6654-treated H358 tumors after 5 days. **B,** Bar graph quantification of SOS1 (left) and pERK (right) at the indicated doses and tumor collection timepoints. **C,** Immunoblot analysis for SOS1, pERK, and ERK after the treatment with BTX-6654 at the indicated doses and collection timepoints. **D,** Antitumor efficacy of BTX-6654 and BI3406 in H358 xenografts for 28 days. **E,** Plasma and tumor analysis from BTX-6654–treated H358 tumors after 28 days. **F,** Bar graph quantification of SOS1 at the indicated doses and tumor collection timepoints. **G,** Immunoblot analysis for SOS1 after treatment with BTX-6654 at the indicated doses and timepoints from H358 tumors. **H,** Antitumor efficacy of BTX-6654 and BI3406 at the indicated doses in MIA PaCa-2 xenografts for 28 days. **I,** Plasma and tumor analysis from BTX-6654–treated MIA PaCa-2 tumors after 28 days. **J,** Bar graph quantification of SOS1 at the indicated doses and tumor collection timepoints. **K,** Immunoblot analysis for SOS1 after treatment with BTX-6654 at the indicated doses and timepoints from MIA PaCa-2 tumors. Data are represented as average ± SEM from 10 mice per group. TGI, tumor growth inhibition. Dotted line is set at 10% SOS1 protein remaining (**B**, **F**, **J**). Vinculin was used as a loading control in immunoblot analysis (**C**, **G**, **K**). Statistical significance was determined with respect to the vehicle group using a two-tailed *t* test (*, $P < 0.05$; **, $P < 0.01$; ***, $P < 0.005$).

degraders in non-SOS1 sensitive GP2D (*KRAS* G12D) cells. Overall, BTX-6654 and BTX-7312 demonstrated synergy with inhibitors acting upstream and downstream of SOS1 across *KRAS*-mutant cell lines.

Next, we investigated whether the combination of sotorasib or trametinib with BTX-6654 could enhance TGI relative to monotherapy in the xMIA PaCa-2 xenograft model. xMiaPaCa-2 cells were established by *in vivo* passaging of MiaPaCa-2 cells to achieve better *in vivo* growth rate. Treatment of BTX-6654 (10 mg/kg, twice daily) and sotorasib (10 mg/kg, once daily) as monotherapy resulted in TGI of 43% and 40%, respectively, whereas the combination significantly improved TGI to 83% ($P < 0.005$) relative to vehicle control (**Fig. 6C**). Similarly, cotreatment with BTX-6654 and trametinib (0.125 mg/kg, twice daily) enhanced TGI to 64% ($P < 0.005$) in xMIA PaCa-2 xenograft model (**Fig. 6D**). Collectively, these data illustrate the ability of SOS1 degraders to synergize with multiple inhibitors to provide enhanced efficacy in cultured cells and xenograft models.

Discussion

The development of bifunctional degraders expands the molecular targeting paradigm beyond classical approaches. The catalytic mechanism of bifunctional degraders can provide higher potency than small-molecule inhibitors (44). Consistent with this, SOS1 degradation afforded more potent inhibition of downstream signaling and cell proliferation than their respective inhibitors. The mechanism for this, however, remains to be elucidated.

Adding the linker and cereblon-ligand to the SOS1 ligand could produce higher-affinity SOS1 binding. However, our results illustrate that both SOS1 degraders and their respective ligands bound with near equal affinity to SOS1 and they demonstrated cereblon-dependent activity, suggesting that enhanced inhibition of SOS1 cannot account for this difference. Alternately, degrading SOS1 might abrogate SOS1 activity mediated by other functional or scaffolding domains not targeted by SOS1 inhibitors. The binding of GTP-bound RAS proteins to the SOS1 allosteric domain can boost SOS1 activity up to 500-fold and is required for tumor growth (13, 17, 45). SOS1 also contains a putative RAC-GEF domain with RAC-GEF activity *in vitro* (16, 31, 46). RAC1 activity is required for tumorigenesis in a *KRAS* G12D-activated mouse model (47). Notably, both the allosteric and RAC-GEF domains are required for the transformative properties of the oncogenic SOS1 mutation N233Y (48). Future structure-function SOS1 analyses may reveal whether removal of these additional roles via degradation can account for the added potency of SOS1 degraders.

While the modes of administration differed between BTX-6654 and BI3406, both compounds exhibited similar TGI in *KRAS* G12C-mutant xenografts. This was a bit surprising considering that BTX-6654 was more potent than its inhibitor-based ligand in cell-based assays. However, a recent study revealed that a VHL-SOS1 inhibitor-based PROTAC (ZZ151) elicited greater TGI than BI-3406 in *KRAS* G12D AsPC-1 xenografts (19). This suggests that SOS1 degradation could allow for better TGI compared with inhibition but may depend upon the presence of specific *KRAS* mutations and additional comutations. Despite the potential context-dependent effects, the similar potencies of BTX-6654 and BI3406 suggests that targeting SOS1 alone produces only a certain level of TGI in *KRAS* G12C-mutant xenografts and could be due to the presence of SOS2. SOS2 might compensate for SOS1 by acting as the GEF to reload KRAS or other RAS proteins. Targeting SOS1 alone reduces pERK and pS6 levels only to approximately 40%–50% suggesting that cotargeting other RAS GEFs (e.g., SOS2, RASGRFs, RASGRPs) might be required to fully suppress these downstream markers. This notion is validated by the fact that degradation or inhibition of SOS1 in combination with genetic SOS2 ablation resulted in deeper growth inhibition in 3D proliferation assays, resulting from enhanced pathway suppression (7). Despite this limitation, BTX-6654 demonstrated that SOS1 degradation could elicit maximal SOS1 targeting as SOS1 inhibition.

While SOS1 degraders demonstrated antiproliferative activity across multiple *KRAS*-mutant cell lines, we observed no sensitivity in *KRAS* G12D-mutant cell lines. Although the slower intrinsic GTP hydrolysis rate for *KRAS* G12D relative to *KRAS* G12C could explain this, SOS1 degraders were active in cell lines with hydrolysis rates slower than *KRAS* G12D, making this explanation unlikely. Despite the fact that previous studies reported antiproliferative effects with SOS1 inhibitors and degraders in *KRAS* G12D-mutant cells (7, 19), sensitivity to SOS1 inhibitors was not observed in our assays, possibly due to differences in methodology. In addition, failure to reduce cell viability in certain *KRAS*-mutant cell lines could be caused by cell-intrinsic resistance to bifunctional degraders via drug efflux driven by high *MDR1* expression (49). However, synergy was observed with allele-specific *KRAS*-mutant inhibitors in SOS1 non-sensitive cell lines (GP2D, SW837, SW1573, NCI-H2030), suggesting that SOS1 degraders cross cell membranes, but SOS1 degradation alone is insufficient to drive antiproliferative activity.

SOS1 degrader activity was not limited to *KRAS*-mutant cancers, but also exhibited antiproliferative effects in *KRAS* WT CML (K562) cells. Analysis of SOS1 dependency in the DepMap portal revealed that SOS1 had the highest dependency score across blood cancer cell lines with an enrichment in CML cell lines (40, 50). Consistent with this, genetic ablation of SOS1 reduced the leukemogenic potential of *BCR-ABL* oncogene and prevented CML development in p210 *BCR/ABL* mice (50, 51). While SOS1 blockade failed to inhibit proliferation in *KRAS* G12D-mutated colorectal or lung cancer cell lines, SOS1 depletion relieved *KRAS* G12D-induced myeloproliferative neoplasm phenotypes and extended survival in mice (52). In addition, exome sequencing analysis has identified oncogenic mutations in SOS1 that drive anchorage-independent growth in cellular models and tumor growth (48). Pharmacologic intervention of SOS1 could provide a meaningful therapeutic response in these SOS1-dependent or -driven cancers. Given the strong dependency on SOS1 and its connection with RAC activity (51), SOS1 degradation could be a more effective strategy over SOS1 inhibition in *BCR-ABL*–driven CML tumor models.

Significantly, using SOS1 degraders could prevent the effects caused by potential secondary mutations that emerge as acquired resistance to RTK-RAS-MAPK pathway inhibitors that result in pathway reactivation, as observed with targeted therapies in *EGFR*- and *KRAS*-mutant tumors (6, 53–55). In such cases, SOS1 could provide added benefit, given its role as a downstream mediator of RTK signaling output. Not only did SOS1 degraders synergize with various pathway inhibitors *in vitro*, but they also provided added efficacy to sotorasib and trametinib in *KRAS* G12C-mutant xenografts. While a low dose of sotorasib was used in our study, we predict that a higher dose of sotorasib with BTX-6654 would produce tumor growth stasis or regression similar to the observed combination with adagrasib and BI-3406 in *KRAS* G12C xenografts (8). The enhanced potency of SOS1 degradation with *KRAS* G12C inhibition likely results in deeper suppression of KRAS-GTP levels and downstream signaling mediated by pathway reactivation of sotorasib. Collectively, our study highlights the potential of SOS1 degradation to provide additional benefits relative to RTK-RAS-MAPK inhibitors.

CRBN-based bifunctional degraders run the risk of also degrading cereblon neosubstrates (56). While our SOS1 degraders were clean for

most neosubstrates, BTX-6654 and BTX-7312 demonstrated degradation of SALL4 (spalt-like transcription factor 4). SALL4 is an embryonic C2H2 zinc finger transcription factor that mediates fetal limb development and is cereblon neosubstrate (34, 57, 58). Degradation of SALL4 is proposed to be one potential cause for thalidomide-induced teratogenicity. While expressed in fetal issues, downregulation of SALL4 after birth results in absent expression except for germline cells in mice and humans (59–61). Despite this, thalidomide and other cereblon-binding therapeutics are clinically approved drugs for the treatment of multiple myeloma. SALL4 expression was not detected in the cancer cell lines used in this study and does not contribute to the potency associated with the SOS1 degraders. Notably, BTX-6654 and BTX-7312 are only being investigated in the preclinical stage.

In summary, we developed cereblon-based degraders that induce potent and selective degradation of SOS1. SOS1 degradation reduced cell viability by inhibiting downstream signaling, both in *KRAS*-mutant cell lines and xenograft mouse models. Importantly, our results highlight the benefit of combining SOS1 degraders with other RTK-RAS-MAPK pathway inhibitors, thereby expanding the therapeutic window for *KRAS*-driven cancers. In addition to *KRAS*-mutant cancers, SOS1 degraders may represent a promising therapeutic option for the treatment of SOS1-dependent or -driven cancers, including hematologic tumors.

Authors' Disclosures

K. Begovich reports a patent for United States Provisional Application No. 63/520,067 pending to BioTheryX, Inc. A. Schoolmeesters reports a patent for United States Provisional Application No. 63/520,067 pending to BioTheryX, Inc. N. Rajapakse reports a patent United States Provisional Application No. 63/520,067 pending to BioTheryX, Inc. E. Martinez-Terroba reports a patent for United States Provisional Application No. 63/520,067 pending to BioTheryX, Inc. B. Whitefield reports a patent for WO2023178130A1 issued. A. Okano reports a patent for United States Provisional Application No. 63/520,067 pending to BioTheryX, Inc. V. Mali reports a patent for United States Provisional Application No. 63/520,067 pending to BioTheryX, Inc. S. Huang reports a patent for United States Provisional Application No. 63/520,067 pending to BioTheryX, Inc. A.H. Chourasia reports a patent for United States Provisional Application No. 63/520,067 pending to BioTheryX, Inc. L. Fung reports a patent for WO2023178130A1 issued. No disclosures were reported by the other authors.

Authors' Contributions

K. Begovich: Conceptualization, data curation, formal analysis, supervision, validation, investigation, visualization, methodology, writing–original draft, project administration, writing–review and editing. **A. Schoolmeesters:** Conceptualization, writing–review and editing. **N. Rajapakse:** Conceptualization, writing–review and editing. **E. Martinez-Terroba:** Conceptualization, writing–review and editing. **M. Kumar:** Conceptualization, writing–review and editing. **A. Shakya:** Conceptualization, writing–review and editing. **C. Lai:** Conceptualization, writing–review and editing. **S. Greene:** Conceptualization, writing–review and editing. **B. Whitefield:** Conceptualization, writing–review and editing. **A. Okano:** Conceptualization, writing–review and editing. **V. Mali:** Conceptualization, writing–review and editing. **S. Huang:** Conceptualization, writing–review and editing. **A.H. Chourasia:** Conceptualization, writing–review and editing. **L. Fung:** Conceptualization, writing–review and editing.

Acknowledgments

The authors thank the staff members of the proteomics core facility at Sanford Burnham Prebys Medical Discovery Institute for their assistance. We thank Ashwini Oke for assistance in generating graphs for proteomic samples. Brandon Whitefield was employed at BioTheryx during the conduct of this study and is currently employed at Innovo Therapeutics. Maneesh Kumar was employed at BioTheryx during the conduct of this study. Editorial support by Stephanie Morgan, PhD, and Robert Rydzewski, MS (Second City Science), was funded by BioTheryx. Finally, we acknowledge all the researchers and employees at BioTheryx who were not listed but worked to make this study possible.

Support for this study and medical writing support were provided by BioTheryx, Inc.

Note

Supplementary data for this article are available at Molecular Cancer Therapeutics Online (http://mct.aacrjournals.org/).

Received August 7, 2023; revised October 12, 2023; accepted January 11, 2024; published first January 15, 2024.

References

1. Lee JK, Sivakumar S, Schrock AB, Madison R, Fabrizio D, Gjoerup O, et al. Comprehensive pan-cancer genomic landscape of KRAS altered cancers and real-world outcomes in solid tumors. NPJ Precis Oncol 2022;6:91.
2. Hunter JC, Manandhar A, Carrasco MA, Gurbani D, Gondi S, Westover KD. Biochemical and structural analysis of common cancer-associated KRAS mutations. Mol Cancer Res 2015;13:1325–35.
3. Ostrem JM, Peters U, Sos ML, Wells JA, Shokat KM. K-Ras(G12C) inhibitors allosterically control GTP affinity and effector interactions. Nature 2013;503:548–51.
4. Hallin J, Engstrom LD, Hargis L, Calinisan A, Aranda R, Briere DM, et al. The KRAS(G12C) inhibitor MRTX849 provides insight toward therapeutic susceptibility of KRAS-mutant cancers in mouse models and patients. Cancer Discov 2020;10:54–71.
5. Lanman BA, Allen JR, Allen JG, Amegadzie AK, Ashton KS, Booker SK, et al. Discovery of a covalent inhibitor of KRAS(G12C) (AMG 510) for the treatment of solid tumors. J Med Chem 2020;63:52–65.
6. Awad MM, Liu S, Rybkin II, Arbour KC, Dilly J, Zhu VW, et al. Acquired resistance to KRAS(G12C) inhibition in cancer. N Engl J Med 2021;384:2382–93.
7. Hofmann MH, Gmachl M, Ramharter J, Savarese F, Gerlach D, Marszalek JR, et al. BI-3406, a potent and selective SOS1-KRAS interaction inhibitor, is effective in KRAS-driven cancers through combined MEK inhibition. Cancer Discov 2021;11:142–57.
8. Thatikonda V, Lu H, Jurado S, Kostyrko K, Bristow CA, Bosch K, et al. Combined KRAS (G12C) and SOS1 inhibition enhances and extends the anti-tumor response in KRAS (G12C) -driven cancers by addressing intrinsic and acquired resistance. bioRxiv 2023.
9. Boriack-Sjodin PA, Margarit SM, Bar-Sagi D, Kuriyan J. The structural basis of the activation of Ras by SOS. Nature 1998;394:337–43.
10. Nichols RJ, Haderk F, Stahlhut C, Schulze CJ, Hemmati G, Wildes D, et al. RAS nucleotide cycling underlies the SHP2 phosphatase dependence of mutant BRAF-, NF1- and RAS-driven cancers. Nat Cell Biol 2018;20:1064–73.
11. Rozakis-Adcock M, van der Geer P, Mbamalu G, Pawson T. MAP kinase phosphorylation of mSos1 promotes dissociation of mSOS1-SHC and mSOS1-EGF receptor complexes. Oncogene 1995;11:1417–26.
12. Depeille P, Henricks LM, van de Ven RA, Lemmens E, Wang CY, Matli M, et al. RasGRP1 opposes proliferative EGFR-SOS1-Ras signals and restricts intestinal epithelial cell growth. Nat Cell Biol 2015;17:804–15.
13. Jeng HH, Taylor LJ, Bar-Sagi D. Sos-mediated cross-activation of wild-type Ras by oncogenic Ras is essential for tumorigenesis. Nat Commun 2012;3:1168.
14. Ketcham JM, Haling J, Khare S, Bowcut V, Briere DM, Burns AC, et al. Design and discovery of MRTX0902, a potent, selective, brain-penetrant, and orally bioavailable inhibitor of the SOS1:KRAS protein-protein interaction. J Med Chem 2022;65:9678–90.
15. Chirnomas D, Hornberger KR, Crews CM. Protein degraders enter the clinic - a new approach to cancer therapy. Nat Rev Clin Oncol 2023;20:265–78.
16. Innocenti M, Tenca P, Frittoli E, Faretta M, Tocchetti A, Di Fiore PP, et al. Mechanisms through which Sos-1 coordinates the activation of Ras and Rac. J Cell Biol 2002;156:125–36.
17. Margarit SM, Sondermann H, Hall BE, Nagar B, Hoelz A, Pirruccello M, et al. Structural evidence for feedback activation by Ras.GTP of the Ras-specific nucleotide exchange factor SOS. Cell 2003;112:685–9.

18. Zhou C, Fan Z, Zhou Z, Li Y, Cui R, Liu C, et al. Discovery of the first-in-class agonist-based SOS1 PROTACs effective in human cancer cells harboring various KRAS mutations. J Med Chem 2022;65:3923–42.
19. Zhou Z, Zhou G, Zhou C, Fan Z, Cui R, Li Y, et al. Discovery of a potent, cooperative, and selective SOS1 PROTAC ZZ151 with *in vivo* antitumor efficacy in KRAS-mutant cancers. J Med Chem 2023;66:4197–214.
20. Bian Y, Alem D, Beato F, Hogenson TL, Yang X, Jiang K, et al. Development of SOS1 inhibitor-based degraders to target KRAS-mutant colorectal cancer. J Med Chem 2022;65:16432–50.
21. Hallin J, Bowcut V, Calinisan A, Briere DM, Hargis L, Engstrom LD, et al. Anti-tumor efficacy of a potent and selective non-covalent KRAS(G12D) inhibitor. Nat Med 2022;28:2171–82.
22. Gilmartin AG, Bleam MR, Groy A, Moss KG, Minthorn EA, Kulkarni SG, et al. GSK1120212 (JTP-74057) is an inhibitor of MEK activity and activation with favorable pharmacokinetic properties for sustained *in vivo* pathway inhibition. Clin Cancer Res 2011;17:989–1000.
23. Li D, Ambrogio L, Shimamura T, Kubo S, Takahashi M, Chirieac LR, et al. BIBW2992, an irreversible EGFR/HER2 inhibitor highly effective in preclinical lung cancer models. Oncogene 2008;27:4702–11.
24. Bjorklund CC, Kang J, Amatangelo M, Polonskaia A, Katz M, Chiu H, et al. Iberdomide (CC-220) is a potent cereblon E3 ligase modulator with antitumor and immunostimulatory activities in lenalidomide- and pomalidomide-resistant multiple myeloma cells with dysregulated CRBN. Leukemia 2020;34:1197–201.
25. Lee DH, Goldberg AL. Proteasome inhibitors: valuable new tools for cell biologists. Trends Cell Biol 1998;8:397–403.
26. Soucy TA, Smith PG, Milhollen MA, Berger AJ, Gavin JM, Adhikari S, et al. An inhibitor of NEDD8-activating enzyme as a new approach to treat cancer. Nature 2009;458:732–6.
27. Huang T, Choi M, Tzouros M, Golling S, Pandya NJ, Banfai B, et al. MSstatsTMT: statistical detection of differentially abundant proteins in experiments with isobaric labeling and multiple mixtures. Mol Cell Proteomics 2020;19:1706–2.
28. Ianevski A, Giri AK, Aittokallio T. SynergyFinder 3.0: an interactive analysis and consensus interpretation of multi-drug synergies across multiple samples. Nucleic Acids Res 2022;50:W739–W43.
29. Arnold MMK JM, Smith CR, Lawson JD, Burns AC, Wang X, et al. Mirati Therapeutics, Inc., assignee. SOS1 Inhibitors patent WO 2021127429. 2021.
30. Cregg JJB A, Aay N, Tambo-ong AA, Koltun ES, Gill AL, et al. Revolution Medicines, Inc., assignee. Bicyclic Heterocyclyl Compounds and Uses Thereof patent WO 2020180770 A1. 2020.
31. Chen PC, Wakimoto H, Conner D, Araki T, Yuan T, Roberts A, et al. Activation of multiple signaling pathways causes developmental defects in mice with a Noonan syndrome-associated Sos1 mutation. J Clin Invest 2010;120:4353–65.
32. Roy RD, Rosenmund C, Stefan MI. Cooperative binding mitigates the high-dose hook effect. BMC Syst Biol 2017;11:74.
33. Nielsen KH, Papageorge AG, Vass WC, Willumsen BM, Lowy DR. The Ras-specific exchange factors mouse SOS1 (mSOS1) and mSOS2 are regulated differently: mSOS2 contains ubiquitination signals absent in mSOS1. Mol Cell Biol 1997;17:7132–8.
34. Donovan KA, An J, Nowak RP, Yuan JC, Fink EC, Berry BC, et al. Thalidomide promotes degradation of SALL4, a transcription factor implicated in duane radial ray syndrome. eLife 2018;7:e38430.
35. Buechler C, Bodzioch M, Bared SM, Sigruener A, Boettcher A, Lapicka-Bodzioch K, et al. Expression pattern and raft association of NIPSNAP3 and NIPSNAP4, highly homologous proteins encoded by genes in close proximity to the ATP-binding cassette transporter A1. Genomics 2004;83:1116–24.
36. Citron BA, Davis MD, Milstien S, Gutierrez J, Mendel DB, Crabtree GR, et al. Identity of 4a-carbinolamine dehydratase, a component of the phenylalanine hydroxylation system, and DCoH, a transregulator of homeodomain proteins. Proc Natl Acad Sci U S A 1992;89:11891–4.
37. Thony B, Neuheiser F, Kierat L, Blaskovics M, Arn PH, Ferreira P, et al. Hyperphenylalaninemia with high levels of 7-biopterin is associated with mutations in the PCBD gene encoding the bifunctional protein pterin-4a-carbinolamine dehydratase and transcriptional coactivator (DCoH). Am J Hum Genet 1998;62:1302–11.
38. Hillig RC, Sautier B, Schroeder J, Moosmayer D, Hilpmann A, Stegmann CM, et al. Discovery of potent SOS1 inhibitors that block RAS activation via disruption of the RAS-SOS1 interaction. Proc Natl Acad Sci U S A 2019;116:2551–60.
39. Singh A, Greninger P, Rhodes D, Koopman L, Violette S, Bardeesy N, et al. A gene expression signature associated with "K-Ras addiction" reveals regulators of EMT and tumor cell survival. Cancer Cell 2009;15:489–500.
40. Dempster JM, Boyle I, Vazquez F, Root DE, Boehm JS, Hahn WC, et al. Chronos: a cell population dynamics model of CRISPR experiments that improves inference of gene fitness effects. Genome Biol 2021;22:343.
41. Bemis TA, La Clair JJ, Burkart MD. Unraveling the role of linker design in proteolysis targeting chimeras. J Med Chem 2021;64:8042–52.
42. Ramharter J, Kessler D, Ettmayer P, Hofmann MH, Gerstberger T, Gmachl M, et al. One atom makes all the difference: getting a foot in the door between SOS1 and KRAS. J Med Chem 2021;64:6569–80.
43. Theard PL, Sheffels E, Sealover NE, Linke AJ, Pratico DJ, Kortum RL. Marked synergy by vertical inhibition of EGFR signaling in NSCLC spheroids shows SOS1 is a therapeutic target in EGFR-mutated cancer. eLife 2020;9:e58204.
44. Burslem GM, Smith BE, Lai AC, Jaime-Figueroa S, McQuaid DC, Bondeson DP, et al. The advantages of targeted protein degradation over inhibition: an RTK case study. Cell Chem Biol 2018;25:67–77.
45. Sondermann H, Soisson SM, Boykevisch S, Yang SS, Bar-Sagi D, Kuriyan J. Structural analysis of autoinhibition in the Ras activator son of sevenless. Cell 2004;119:393–405.
46. Nimnual AS, Yatsula BA, Bar-Sagi D. Coupling of Ras and Rac guanosine triphosphatases through the Ras exchanger Sos. Science 1998;279:560–3.
47. Kissil JL, Walmsley MJ, Hanlon L, Haigis KM, Bender Kim CF, Sweet-Cordero A, et al. Requirement for Rac1 in a K-ras induced lung cancer in the mouse. Cancer Res 2007;67:8089–94.
48. Cai D, Choi PS, Gelbard M, Meyerson M. Identification and characterization of oncogenic SOS1 mutations in lung adenocarcinoma. Mol Cancer Res 2019;17:1002–12.
49. Kurimchak AM, Herrera-Montavez C, Montserrat-Sangra S, Araiza-Olivera D, Hu J, Neumann-Domer R, et al. The drug efflux pump MDR1 promotes intrinsic and acquired resistance to PROTACs in cancer cells. Sci Signal 2022;15:eabn2707.
50. Gomez C, Garcia-Navas R, Baltanas FC, Fuentes-Mateos R, Fernandez-Medarde A, Calzada N, et al. Critical requirement of SOS1 for development of BCR/ABL-driven chronic myelogenous leukemia. Cancers 2022;14:3893.
51. Gerboth S, Frittoli E, Palamidessi A, Baltanas FC, Salek M, Rappsilber J, et al. Phosphorylation of SOS1 on tyrosine 1196 promotes its RAC GEF activity and contributes to BCR-ABL leukemogenesis. Leukemia 2018;32:820–77.
52. You X, Kong G, Ranheim EA, Yang D, Zhou Y, Zhang J. Unique dependence on Sos1 in Kras (G12D) -induced leukemogenesis. Blood 2018;132:2575–9.
53. Pao W, Chmielecki J. Rational, biologically based treatment of EGFR-mutant non-small-cell lung cancer. Nat Rev Cancer 2010;10:760–74.
54. Tanaka N, Lin JJ, Li C, Ryan MB, Zhang J, Kiedrowski LA, et al. Clinical acquired resistance to KRAS(G12C) inhibition through a novel KRAS switch-II pocket mutation and polyclonal alterations converging on RAS-MAPK reactivation. Cancer Discov 2021;11:1913–22.
55. Warren HR, Ross SJ, Smith PD, Coulson JM, Prior IA. Combinatorial approaches for mitigating resistance to KRAS-targeted therapies. Biochem J 2022;479:1985–97.
56. Costacurta M, He J, Thompson PE, Shortt J. Molecular mechanisms of cereblon-interacting small molecules in multiple myeloma therapy. J Pers Med 2021;11:1185.
57. Akiyama R, Kawakami H, Wong J, Oishi I, Nishinakamura R, Kawakami Y. Sall4-Gli3 system in early limb progenitors is essential for the development of limb skeletal elements. Proc Natl Acad Sci U S A 2015;112:5075–8.
58. Matyskiela ME, Couto S, Zheng X, Lu G, Hui J, Stamp K, et al. SALL4 mediates teratogenicity as a thalidomide-dependent cereblon substrate. Nat Chem Biol 2018;14:981–7.
59. Eildermann K, Aeckerle N, Debowski K, Godmann M, Christiansen H, Heistermann M, et al. Developmental expression of the pluripotency factor sal-like protein 4 in the monkey, human and mouse testis: restriction to premeiotic germ cells. Cells Tissues Organs 2012;196:206–20.
60. Kohlhase J, Heinrich M, Schubert L, Liebers M, Kispert A, Laccone F, et al. Okihiro syndrome is caused by SALL4 mutations. Hum Mol Genet 2002;11:2979–87.
61. Miettinen M, Wang Z, McCue PA, Sarlomo-Rikala M, Rys J, Biernat W, et al. SALL4 expression in germ cell and non-germ cell tumors: a systematic immunohistochemical study of 3215 cases. Am J Surg Pathol 2014;38:410–20.